Comparative connectomics of two distantly related nematode species reveals patterns of nervous system evolution

Steven J. Cook[1*#], Cristine A. Kalinski[1], Curtis M. Loer[2], Nadin Memar[3], Maryam Majeed[1#], Sarah Rebecca Stephen[1], Daniel J. Bumbarger[4], Metta Riebesell[4], Ralf Schnabel[3], Ralf J. Sommer[4] and Oliver Hobert[1*]

Running title: Mind of a predatory worm

[1] Department of Biological Sciences, Columbia University; Howard Hughes Medical Institute, New York, NY

[2] Department of Biology, University of San Diego, San Diego, CA

[3] Institut für Genetik, Technische Universität Braunschweig, Germany

[4] Max-Planck Institute for Biology Tübingen, Department for Evolutionary Biology, Tübingen, Germany

[#]Current Address: Allen Institute for Brain Science, Seattle, WA

*Corresponding authors:

E-mail: steven.cook@alleninstitute.org (SJC), or38@columbia.edu (OH)

Abstract

Understanding the evolution of the bilaterian brain requires a detailed exploration of the precise nature of cellular and subcellular differences between related brains. To define the anatomical substrates of evolutionary change in the nervous system, we undertook an electron micrographic reconstruction of the brain of the predatory nematode *Pristionchus pacificus.* A comparison with the brain of *Caenorhabditis elegans*, which diverged at least 100 million years ago, reveals a conserved nematode core connectome and a wide range of specific substrates of evolutionary change. These changes include differences in neuronal cell death, neuronal cell position, axo-dendritic projection patterns and many changes in synaptic connectivity of homologous neurons that display no obvious changes in overall neurite morphology and projection patterns. Differences in connectivity are distributed throughout the nervous system arguing against specific hot spots of evolutionary change and extend to differences in neuro/glia connectivity. We observed examples of apparent circuit drift, where changes in morphology and connectivity of a neuron do not appear to alter its behavioral output. In conclusion, our comprehensive comparison of distantly related nematode species provides novel vistas on patterns of conservation as well as the substrates of evolutionary change in the brain that span multiple organizational levels.

Brains have undergone dramatic changes across animal evolution, evidenced by elaborations and increases in size, anatomical complexity and functional capacities. Due to anatomical complexity and difficulties associated with identifying homologous neurons, the precise natures of evolutionary changes is often hard to pinpoint with cellular or synaptic resolution in vertebrate brains. However, in organisms with numerically more constrained and anatomically well-described brains, identifying homologous neurons is more feasible, which permits the delineation of the precise substrates of anatomical change in the brain. Such analysis can address a host of key questions (ROBERTS *et al.* 2022): What are the precise substrates of evolutionary change (e.g., neuron gain or loss; changes in neuronal soma migration patterns; changes in projection patterns; synaptic connectivity changes)? Do some types of changes happen more often than others? Are specific types of changes homogenously distributed across the network or are there specific hotspots of evolutionary changes (e.g., is the sensory periphery of an animal more evolvable than central circuits)?

The nematodes *Pristionchus pacificus* and *Caenorhabditis elegans* are thought to have diverged more than 100 million years ago (QING *et al.* 2023). While this substantial divergence is not immediately obvious based on the overall size or morphology of these species, it shows on many other levels. On a molecular level, the *P. pacificus* genome is 70% larger than the *C. elegans* genome, contains 30% more genes and only roughly 30% of its genes have 1:1 orthologs in *C. elegans* (ATHANASOULI et al. 2020). The divergence of these two nematode species is also apparent in their adaptation to distinct ecological niches and in unique adaptions in sensory, locomotory and feeding behavior (HONG AND SOMMER 2006; SRINIVASAN *et al.* 2008; KROETZ *et al.* 2012). The most striking of these adaptations is the predatory feeding behavior that *P. pacificus* displays toward other nematodes and an associated self-recognition system that prevents cannibalism against kin (RAGSDALE *et al.* 2013; LIGHTFOOT *et al.* 2019).

The many cataloged differences between *P. pacificus* and *C. elegans,* particularly on the behavioral level, prompt the question to what extent the nervous system of these two species has diverged. Previous studies using serial section electron microscopy described differences in the sensory periphery of these worms (i.e., the exposed ciliated ending of these two species) and in the small and isolated nervous system of the foregut ("pharynx") (BUMBARGER *et al.* 2013; HONG *et al.* 2019). We analyzed to what extent the entire centralized brain - the cluster of head ganglia that controls many complex nematode behaviors - has

diverged among these two distant nematode species. We expected that such analysis might identify and provide a panoramic view of the substrates of evolutionary change, thereby addressing several questions that only a broad, brain-wide comparative connectomic analysis can answer.

Nanoscale reconstruction of the *P. pacificus* nervous system

We analyzed serial section electron microscopy of two adult hermaphrodite *P. pacificus* heads from the anterior nose tip to the retrovesicular ganglion, including the nerve ring, the major neuropil of nematodes (**Figure 1A**). We reconstructed the ultrastructure of all neurons in these two animals, analyzed the extent of the membrane contacts between their neurites (the "contactome") (**Supplement Data 1,2**) and their patterns of chemical synaptic connectivity ("connectome") **(Supplement Data 3,4**). Based on remarkably well-conserved cell body position as well as characteristic features of neurite trajectories and placement within fascicles, we were able to clearly assign homology to all neurons found in the *C. elegans* head (**Figure 1B; Figure 1 Supplement 1** contains renderings of all neurons). Such clear one-to-one homology assignments are difficult to make upon comparison of more complex nervous systems and present a unique advantage of the nematode phylum with its limited cellular complexity and apparent stereotypy of cellular composition and lineage. These neuronal homology assignments allowed us to ask if - and to what extent - homologous neurons have evolved distinct features. In the ensuing sections of this manuscript, we describe the distinct patterns of evolutionary changes that we observed.

Differences in neuronal composition and location

We found one *C. elegans* interneuron class, the bilaterally symmetric AVH neuron pair, to be missing in *P. pacificus*. This neuron pair is stereotypically located in the lateral ganglion in *C. elegans,* from where it extends a neurite through the nerve ring into and along the ventral nerve cord (WHITE *et al.* 1986). The sister cells of both left and right AVH neurons undergo programmed cell death in *C. elegans* (SULSTON et al. 1983)(**Figure 1C, Figure 1 Supplement 2A**). Tracing the lineage of embryonic cell division in *P. pacificus* using 4D video microscopy (SCHNABEL et al. 1997), we found that this cell death occurs one cell division earlier, hence explaining the absence of AVHL/R in *P. pacificus* **(Figure 1C,D;**

Figure 1 Supplement 2B). Our embryonic lineaging analysis also reveals that precocious cell death can explain the previously noted absence of the pharyngeal gland cell g2 in *P. pacificus* (RIEBESELL AND SOMMER 2017). As in the case of AVH, the sister of g2 dies in *C. elegans*, while in *P. pacificus,* the mother dies (**Figure 1 Supplement 3A-D**). Hence, together with the previously reported excess cell death of a subset of VC ventral cord motorneurons in *P. pacificus* (EIZINGER et al. 1999), alterations in the spatial and temporal specificity of programmed cell death appear to constitute a recurrently used mechanism for shaping species-specific nervous system composition.

We traced the lineage of AVH in two more distantly related nematodes that can serve as outgroups to *P. pacificus* and *C. elegans*, *Acrobeloides nanus* and *Plectus sambesii,* and observed that in both species the cleavage pattern of the AVH-generating lineage (as well as the g2 gland-generating lineage) resembles the *C. elegans* pattern. In both species the sister, rather than the mother, of the presumptive AVH neuron and g2 gland cell undergoes programmed cell death (**Figure 1 Supplement 2, 3**). These observations indicate that the loss of *P. pacificus* AVH (as well as g2) due to the heterochronic death of the mother cell is a derived feature.

We observed a remarkable molecular correlation to the loss of AVH neurons in *P. pacificus.* In *C. elegans*, the AVH neurons require a divergent member of the bHLH-PAS family of transcription factors, *hlh-34*, for their proper differentiation (BERGHOFF *et al.* 2021; COOK *et al.* 2021). Sequence surveys of multiple highly divergent nematode species with complete and well-annotated genomes shows that the *hlh-34* locus is lost in the *Pristionchus* genus (**Figure 1 Supplement 2C**). Hence, the loss of a neuron is correlated with the genomic loss of its identity regulator.

We asked whether the loss of AVH in *P. pacificus* is accompanied by synaptic wiring changes in a neighboring neuron, AVJ, that shares many anatomical similarities to AVH. In *C. elegans* both neurons display a similar neurite extension pattern through the nerve ring and along the ventral cord (WHITE *et al.* 1986). The two neurons are electrically coupled and share some synaptic partners (WHITE *et al.* 1986; COOK *et al.* 2019; WITVLIET *et al.* 2021). However, we do not observe that the synaptic contacts normally specifically made by AVH and not AVJ are absorbed by *P. pacificus* AVJ. Instead, AVJ generates additional novel, *P. pacificus*-specific synapses (**Figure 3 Supplement 2**).

Differences in neuronal location

Another type of evolutionary change concerns cell soma position. Generally, the relative positions of homologous neuronal somas are highly conserved between *P. pacificus* and *C. elegans*. Notable exceptions are the inner labial, dorsal and ventral IL2 (IL2D and IL2V) sensory neuron pairs. In *C. elegans,* the IL2D and IL2V neuronal soma are located at a similar position along the longitudinal axis in the anterior ganglion as the lateral IL2 neuron pair (WHITE *et al.* 1986). In *P. pacificus,* however, the IL2D and IL2V soma pairs are positioned much more anteriorly (**Figure 1B**). Their axons therefore need to take a much longer path to reach the nerve ring, a feat that they achieve by close fasciculation with inner labial IL1 neurons, whose position is unchanged relative to *C. elegans* (**Figure 1 Supplement 5**). The more anterior localization of the IL2D/V soma means that their dendrites are substantially shortened. Since the IL2D/V dendrites in *C. elegans* make extensive dendritic branches at the dauer stage to respond to mechanosensory touch involved in nictation behavior (LEE *et al.* 2012; SCHROEDER *et al.* 2013), such shortening may result in a reduced sensory perceptive field of the branched IL2D/V dendrites in nictating *P. pacificus* dauer stage animals.

Differences in neurite projection patterns alter information flow

Many individual neurons display highly characteristic neurite projection or branching patterns in *C. elegans,* which we leveraged to describe similarities and differences across species. For example, the *C. elegans* AIB neurites display an abrupt neighborhood shift in the nerve ring (WHITE *et al.* 1986) which is conserved in *P. pacificus* (**Figure 1 Supplement 1**)(HONG *et al.* 2019). Similarly, the unusual, truncated dendrite of the amphid-associated *C. elegans* AUA neuron class (WHITE *et al.* 1986) is also conserved in *P. pacificus* (**Figure 1 Supplement 1**). The ring interneurons RIM, RIH, RIS and RIR display characteristic branching patterns in the *C. elegans* nerve ring and these patterns are also similar in both species (**Figure 1 Supplement 1**). Paralleling these notable patterns of conservation, we discovered a rich set of evolutionary diversifications of projection patterns; several of them resulting in striking differences in presumptive information flow in the two nervous systems. Among the most dramatic differences is an apparently complete repurposing of adult URB

neuron function. In *C. elegans*, all available EM constructions, as well as reporter genes, show that URB extends a long dendrite toward the tip of the nose along the lateral amphid sensory dendrite bundle and extends an axon into the nerve ring to synapse with distinct sensory, inter- and motorneuron classes (WHITE *et al.* 1986; COOK *et al.* 2019; WITVLIET *et al.* 2021). In striking contrast, no dendritic extension of URB neurons is observed in either of the two *P. pacificus* samples (**Figure 2A, Figure 1 Supplement 1**). Moreover, unlike in *C. elegans,* the *P. pacificus* URB axon innervates the head muscles in adults (**Figure 2 Supplement 1A**)**.** The concordant loss of dendrite and rewiring of axonal output suggests a functional switch from sensory to motorneuron between these two species.

Altered neurite extension patterns within the lateral nerve also indicate a divergence of routes of synaptic communication in the two nematode species. In *C. elegans,* the PVD sensory neuron extends a primary dendrite that typically terminates before reaching the nerve ring (WHITE *et al.* 1986; COOK *et al.* 2019). In marked contrast, in both *P. pacificus* samples, this dendrite projects further anteriorly into the nerve ring where it synapses onto AVD and AVJ and receives inputs from the nociceptive ADL neuron (**Figure 2B, Figure 2 Supplement 1B**). Hence, the PVD neurite, normally purely dendritic in *C. elegans,* is repurposed to become axodendritic in *P. pacificus*, thus allowing the lateral nerve to provide ascending input to the brain.

Conversely, the harsh touch mechanoreceptive neuron, FLP, has a shorter axon in *P. pacificus*. In *C. elegans,* the two FLP neurons extend their axons through the deirid commissure, then project into the nerve ring where they generate synaptic outputs to the pre-motor command interneuron AVA (WHITE *et al.* 1986; COOK *et al.* 2019; WITVLIET *et al.* 2021). In *P. pacificus,* the FLP axons terminate before the nerve ring resulting in a loss of connections to the backward movement-inducing AVA while making new connections to the forward movement-inducing PVC command interneuron are generated (**Figure 1 Supplement 3**). While the precise function of FLP in *P. pacificus* is unknown, altering its output from AVA to PVC suggests a repurposing from avoidance to attractive responses to head touch. This change may relate to the predatory behavior of *P. pacificus*, in which contact with prey may not elicit an escape response.

While predatory feeding behavior is the most striking behavioral trait of *P. pacificus*, many aspects of its neural control remain unresolved. In both species, the only neuron to synaptically connect the somatic and pharyngeal nervous systems is RIP (WHITE *et al.* 1986;

BUMBARGER *et al.* 2013; COOK *et al.* 2019; WITVLIET *et al.* 2021). At all developmental stages, the posteriorly directed neurite of RIP is strictly dendritic in the nerve ring of *C. elegans*, assembling synaptic input from a variety of different central neuron classes (WITVLIET *et al.* 2021). In *P. pacificus,* the posteriorly directed RIP neurite extends more deeply into the nerve ring and generates synaptic outputs onto a variety of neuron types (**Figure 2C**). Hence, synaptic information flow through RIP appears unidirectional in *C. elegans* (from nerve ring to the enteric nervous system)*,* while in *P. pacificus*, RIP undergoes a partial polarity change to directly synapse onto both the somatic and enteric nervous systems. It will be interesting to see whether this rewiring relates to the predatory feeding behavior displayed by *P. pacificus.*

The unpaired AQR neuron, an oxygen-sensing neuron exposed to internal body cavities in both species, undergoes another type of striking projection change. In *C. elegans,* the AQR neurite bifurcates upon entry into the nerve ring to extend symmetric neurites along either side of the nerve ring which then terminates shortly before reaching the dorsal midline (**Figure 2D**)(WHITE *et al.* 1986; WITVLIET *et al.* 2021). In neither of the two *P. pacificus* series does the neurite of AQR bifurcate; instead, a single neurite reaches across the dorsal midline to the other side of the nerve ring (**Figure 2D**). The *P. pacificus* AQR neuron makes three small branches not observed in *C. elegans* as well as a large swelling at the dorsal midline, resulting in a preservation of distinctive gap junctions to the PVP neuron, as observed in *C. elegans* (WHITE *et al.* 1986)**(Figure 1 Supplement 1**)**.** However, the *P. pacificus* AQR neuron does not innervate pre-motor command interneurons AVB and AVD, suggesting that AQR activation may trigger distinct behavioral read-outs. Indeed, oxygen-induced behavioral responses appear to be different in *P. pacificus* and *C. elegans* (MORENO *et al.* 2016).

The ASJ amphid sensory neurons display another type of projection change. ASJ neurons in both *C. elegans* and *P. pacificus* have a bipolar morphology with a sensory dendrite to the tip of the nose and an axon into the nerve ring. In *P. pacificus*, both ASJ neurons extend an additional short, thick neurite at or near the soma, not directed toward a specific fascicle but extending along amphid cell bodies **(Figure 2E)**. Strikingly, in both samples and on both sides of the animal, this short neurite is filled with dense core vesicles (**Figure 2 Supplement 1C**), indicating that in *P. pacificus* this neuron has the additional capacity to broadcast neuropeptidergic signals across the nervous system.

Changes in projection patterns do not necessarily result in changes in information flow. The two anterior light touch receptor neuron classes ALM and AVM are electrically coupled,

and each innervates command interneurons to signal reversal behavior in *C. elegans* (CHALFIE *et al.* 1985; WHITE *et al.* 1986). The ventrally located AVM projects a bifurcating axon into the *C. elegans* nerve ring, where synapses are made to command interneurons, and terminates after meeting branches that are sent by lateral ALM touch sensory neurons into the nerve ring (**Figure 2F**)(WHITE *et al.* 1986; WITVLIET *et al.* 2021). In marked contrast, the AVM neuron does not send a bifurcating branch into the *P. pacificus* nerve ring (**Figure 2F**), resulting in the loss of many AVM synapses observed in the adult *C. elegans*. However, the *P. pacificus* ALM neurites instead project further ventrally and posteriorly in *P. pacificus* to reach the unbranched AVM neurite on the ventral side (**Figure 2F**), generating the same large gap junction connection to AVM as they do in *C. elegans* (**Figure 2 Supplement 1D**). In aggregate, synaptic outputs of the ALM and AVM neuron classes to command interneuron are therefore preserved in both nematodes, which is manifested by a similar gentle touch response in both species.

Synaptic connectivity repatterning without obvious changes in neurite projection.

We discovered extensive evolutionary changes in synaptic connectivity patterns in the nerve ring independent of any obvious changes in overall neuron morphology. The elucidation of multiple *C. elegans* connectomes across development indicates a large degree of variability in synaptic connectivity patterns (WITVLIET *et al.* 2021). To account for such variability in the context of interspecies comparisons, we first extracted all synaptic connections that are completely conserved in all 10 available *C. elegans* samples covering multiple larval and adult stages and our two adult *P. pacificus* samples. These connections define a “core connectome” that is conserved across both development and evolution. In addition, we identified connections that are conserved in both *P. pacificus* samples but absent from all 10 *C. elegans* samples (*P. pacificus*-specific connectome) and connections that are absent in both *P. pacificus* samples but present in all 10 *C. elegans* samples (*C. elegans*-specific connectome). These sets of synaptic classifications are illustrated in (**Figure 3A-D)**. Schematic connectivity diagrams of each individual neuron are assembled in **Figure 1, Supplement 2.**

We find that 88% of all neuron classes contribute to the “core nematode connectome” observed in every available EM sample from both species, independent of developmental

stage. The core connectome is not biased to a specific part of the nervous system, i.e., it includes sensory, inter- and motorneurons and extends from the sensory periphery via interneuronal layers to various motor outputs (**Figure 3**). Conversely, neurons that do not form any "core nematode connections" (AVH, AVL, CAN, FLP, PVR, PVT, RID, and SIB) fall into multiple functional categories and are also not biased to a specific part of the nervous system.

Species-specific synaptic connections are also not limited to a specific part of the nervous system, such as its sensory periphery, but are rather distributed throughout the entire connectome. We evaluated the set of neurons born embryonically and found that 72% of the neuron classes that display *C. elegans*-specific connections also generate *P. pacificus*-specific synapses (**Figure 3 Supplement 1**). An additional 5 neurons (AVL, PVR, PVT, RID, SIB) are not connected in the core wiring diagram. Conversely, 68% and 94% of neurons that make *P. pacificus* and *C. elegans*-specific connections also make a core connection, respectively. Species-specific synapses account, on average, for only 15.6% of the synaptic connections of each neuron (**Figure 3 Supplement 1**). Only four neuron classes, ALA, ASJ, RID, and SIA, do not form any species-specific synapses (**Figure 3C,D, Figure 3 Supplement 2**). Other signaling capacities of these two neurons, indicated by the DCV-filled *P. pacificus*-specific extension of ASJ (see above), may have diverged between these two species.

Synaptic wiring changes as a function of neighborhood changes

Species-specific synapses of morphologically similar neurons can be generated by dramatic shifts in neurite neighborhood shifts. The most striking example is the polymodal, nociceptive ASH neuron. In *C. elegans,* the axon of ASH extends medially through the nerve ring, making ample *en passant* contacts with several interneurons, most notably command interneurons, until it meets its contralateral homolog at the dorsal midline (**Figure 4A, Figure 1 supplement 1**). The synaptic output of ASH transforms ASH-sensed nociceptive stimuli into a reversal response via pre-motor command interneurons (KAPLAN AND HORVITZ 1993). Like in *C. elegans,* each ASH axon in *P. pacificus* also extends through the nerve ring to meet its contralateral homolog at the midline, but the path taken through the nerve ring is dramatically different as it mostly travels along the outer side of the nerve ring (**Figure 4B**).

This dramatic difference in neighborhood has substantial consequences on the *en passant* synaptic connectivity: ASH loses its direct output to the homologs of the backward locomotion-inducing command interneurons in *P. pacificus* (**Figure 4C**). These differences in synaptic connectivity are particularly remarkable in light of the experimental finding that in *P. pacificus,* the ASH neurons also mediate reversal to nociceptive stimuli as in *C. elegans* (SRINIVASAN et al. 2008). Hence, in these two nematodes, nociceptive sensory information is perceived by the same neuron but appears to be relayed through different synaptic pathways to produce similar motor outputs.

If neuronal neighborhood shifts are not common, how widespread are species-specific are small neighborhood rearrangements and do they instruct species-specific connections? Several above-mentioned extreme examples of changes in morphology (e.g. ASH, PVD or RIP) produce species-specific adjacencies associated with species-specific connectivity. In total, there are 94 instances of species-specific synaptic connections due to adjacencies that are exclusive to one specific species (**Figure 4 Supplement 1A,B).**

We undertook a more quantitative, whole-brain analysis of the relationship and conservation of neurite adjacency and synaptic connectivity. We found that neuronal adjacency between neuron pairs is generally more highly conserved across all *C. elegans* and *P. pacificus* samples than synaptic connectivity (**Figure 4D,E, Figure 4 Supplement 1B**). The same trend is found in an even more conservative comparison is made by comparing the adjacency (**Figure 4F**) and directed connectivity of only adult samples (**Figure 4G, Figure 4 Supplement 1A,B**). Together, these results show that neuronal adjacency is a more conserved feature of nervous system structure than connectivity.

A previous analysis of neurite adjacency and synaptic connectivity revealed that the relative amount of neurite membrane adjacency predicts synaptic connections between neuron pairs in *C. elegans* (COOK et al. 2023). Consistent with this finding, we found that neuron pairs with species-specific connections show greater mean-scaled adjacencies within the species where the connection is found (**Figure 4G**). For core connections, i.e., neuron pair connections that are conserved between the species, a smaller inter-species difference in mean scaled adjacency is observed (**Figure 4H**). This trend extends to synaptic connectivity, where we observed that the largest connections, on average, are ‘core’. Variable connections are on average, smaller than those found in one species (**Figure 4I**). Taken together, our analysis indicates that changes in neurite adjacency strongly contribute

to creating species-specific synaptic connectivity.

Synaptic connectivity can be accurately modeled using relative adjacency in *C. elegans* (COOK et al. 2023). To explore whether the relationships between connectivity and adjacency are conserved, we extended this modeling approach to *P. pacificus.* We adjusted the training (*C. elegans* contact and connectomes) and test data (*P. pacificus* contact and connectomes), and used two predictors (mean scaled adjacency and brain strata)(BRITTIN *et al.* 2021) to classify synaptic connectivity (present in at least one sample). We found a moderately strong relationship between mean scaled adjacency and mean connection weight among neuron pairs within or across the same brain strata. (**Figure 4 Supplement 2A,B**) (COOK et al. 2023). Our modeling approach yielded superior results across classification algorithms (**Figure 4 Supp.1C**) compared to our previous results modeling connectivity in *C. elegans* alone. For comparative purposes, we plotted the Received Operator and Precision Recall curves for the Logistic Regression classifier, revealing they both could accurately predict connectivity from simple neuronal adjacency characteristics (**Figure 4 Supplement 2D, E**). The striking similarity of results from our modeling across species supports our previous proposal that the control of relative adjacency is a guiding principle of synaptic organization in nematodes (COOK et al. 2023).

Glia connectivity as a substrate of evolutionary change.

We analyzed the other main component of nervous systems, glial cells. The ultrastructure of *P. pacificus* head glia supports a one-to-one correspondence of the three major cell types (sheath, socket, and GLR) (**Figure 5A,C,E**). Despite anatomical similarity, we discovered one novel feature of *P. pacificus* GLR glia, microglia-like cells that extend two types of processes in both species: thin, leaf-like posterior processes that wrap the interior of the muscle-neuron plates of the nerve ring as well as anterior processes that fasciculate with inner labial dendritic sensory fascicles. (**Figure 5C,F**)(HONG *et al.* 2019). Strikingly, in *P. pacificus,* these anterior extensions contain bona fide presynaptic features, e.g., swellings, active zones and synaptic vesicles (**Figure 5G**). The GLR cells receive synaptic input from RIP in both species but make *P. pacificus*-specific output onto inner- and outer labial cells, other glia and the pharyngeal epithelium (**Figure 5H**). So-called “gliotransmission” has been reported in vertebrate astrocytes (SAVTCHOUK AND VOLTERRA 2018) but has not yet been

revealed as a substrate of evolutionary change in a nervous system. As we already speculated in the context of the intriguing wiring differences of the RIP neurons, the ability of *P. pacificus* GLR glia to communicate with pharyngeal tissue may relate to predatory feeding behavior.

We discovered that the astrocyte-like CEPsh glia also display striking changes in synaptic connectivity. The extensions of the CEPsh glia that line the nerve ring are innervated by the neurites of several distinct neuron types in the *C. elegans* nerve ring (WITVLIET *et al.* 2021). Like the GLR glia, the *P. pacificus* CEPsh glia are localized to nearly identical anatomical locations with no gross shift in neighborhood placement. In *P. pacificus*, several of these inputs are lost and others are gained. For example, there is now strong innervation of the CEPsh glia by the AWC olfactory neurons in the nerve ring (**Figure 5B,C,D**). Vertebrate astrocytes also receive synaptic inputs that is translated into gliotransmitter release (SAVTCHOUK AND VOLTERRA 2018). While we observe no obvious synaptic release sites in the CEPsh glia, we note that at least in *C. elegans*, the CEPsh glia release neuropeptides to control stress resistance and animal lifespan (FRAKES *et al.* 2020). If this CEPsh function is preserved in *P. pacificus*, a rewiring of CEPsh glia indicates that the neuronal control of such important physiological parameters may be subject to evolutionary change.

Conclusions

The exceptionally well-described neuronal anatomy of *C. elegans* combined with our analysis of multiple *P. pacificus* datasets yields a comprehensive map of how brains change over millions of years of evolution. Our analysis revealed multi-tiered substrates of evolutionary change, ranging from alteration in the number of individual constituent neurons (exemplified by species-specific neuronal cell death), cell body position, projection patterns of dendrites and/or axons, and changes in synaptic connectivity.

Brain development in vertebrate and invertebrate animals, including nematodes, involves substantial amount of cell death (HENGARTNER AND HORVITZ 1994; FRICKER *et al.* 2018). The discovery of alterations in the cellular specificity of neuronal cell death programs in *C. elegans* and *P. pacificus* indicates that programmed cell death may constitute an important and previously underappreciated driving force in shaping circuit architecture over evolutionary timescales.

Additionally, changes in synaptic connectivity are largely, but not exclusively, the result of changes in relative process adjacency, which provides an additional support toward the applicability of Peters' Rule for the generation of synaptic specificity in nematodes (COOK *et al.* 2023). We speculate that at least some of the changes in circuit architecture relate, in particular, the rewiring of RIP, to the intriguing predatory behavior that *P. pacificus* can engage in.

We also discovered that changes in network structure do not necessarily result in behavioral changes, as illustrated by the ASH sensory neurons which, based on their synaptic connectivity, appear to transmit sensory information to a distinct set of downstream interneurons. Yet, in both species, ASH triggers nociceptive responses to aversive cues (KAPLAN AND HORVITZ 1993; SRINIVASAN *et al.* 2008). Akin to the concept of developmental systems drift (TRUE AND HAAG 2001), the ASH circuit may constitute an example of "circuit drift", in which the pathways of information processing may have drifted, while keeping behavioral output constant (KATZ 2016; ROBERTS *et al.* 2022).

Apart from revealing the specific substrates of evolutionary change, the analysis of whole brains (rather than isolated parts) permitted us to address the fundamental question of whether evolutionary changes homogenously distribute across the network or are concentrated at specific hotspots, such as the sensory periphery. Our analysis demonstrates that evolutionary conservation of synaptic connectivity and evolutionary novelty are distributed throughout the entire brain.

METHODS

EM analysis methodology

Two serial section EM series of eurystomatous (predatory) hermaphrodite animals (BUMBARGER *et al.* 2013) from the PS312 strain were further reconstructed for ultrastructural morphology and connectivity using TrakEM2 (CARDONA *et al.* 2012). From these series, ROIs were created which correspond to the nerve ring and surrounding neuropil. We limited our comparative analysis of neuronal and adjacency to this ROI, but report the connectivity data in **Supplement Data 1,2**. Neural adjacency data for *P. pacificus* were extracted as previously described (BRITTIN *et al.* 2021), with slight modification to extract 'areatree' annotations using multiprocessing. We identified chemical synapses and gap junctions between neurons and tissues using criteria established previously (WHITE *et al.* 1986; COOK *et al.* 2019), but excluded gap junction connectivity from our comparative analysis due to ultrastructural ambiguity within and between species. Connectivity data were extracted using a combination of built-in tools from TrakEM2 and custom parsing scripts. These extracted connectivity data include the number of synapses and weight metric (number of consecutive serial sections where synaptic specializations observed). Our analysis is limited to the number of connections between two neurons unless noted otherwise.

We limited our cross-species comparison of ultrastructure to normal *C. elegans* development and only the hermaphrodite sex. Given its rich description of inter-individual variability, we used anatomical landmarks of *C. elegans* as a reference. To identify neuronal identities, we progressively classified cells based on their morphology (soma location, size, number and direction of processes, hallmark identity features) as previously described (WHITE *et al.* 1986; COOK *et al.* 2019). Further ambiguities were resolved by evaluating the specific location of a process within the neuropil as well as distinct swellings in axons or dendrites. We avoided the use of synaptic connectivity to identify cells. All neuronal cells with connected somas were identified within our region of interest (ROI). However, because the EM series did not cover the entire animal, we were unable to positively identify all processes within the ROI and, therefore, excluded those from our analysis. These cells include 'unknown' RVG neurons that project into the ventral ganglion, which do not have homologous counterparts in *C. elegan*s. Additionally, there are axons that project from the posterior of the animal into the nerve ring but lack distinguishing characteristics in *P. pacificus* which are

seen in *C. elegans*, such as prominent neighborhood positions or distinct branching patterns. For example, there is a bilateral pair of *P. pacificus* axons in the same neighborhood as HSN in *C. elegans*, but these neurons are unbranched, and no *P. pacificus* neuron projects through the left fascicle similar to *C. elegans* HSNL. This observation matches serotonin staining patterns which reveal no obvious HSN candidate in *P. pacificus* (LOER AND RIVARD 2007).

The pharyngeal and amphidial circuits were previously homologized with a 1:1 correspondence between each species in their neuronal identity (BUMBARGER *et al.* 2013; HONG *et al.* 2019). Due to details of their axonal projection patterns, the analysis of reporter data and discussions with R. Hong, we exchange the identities of *P. pacificus* ASE and AWC in this paper relative to a previous analysis of the amphid circuitry of *P. pacificus* (HONG *et al.* 2019). To make accurate morphological comparisons, we evaluated the morphology of P. pacificus neurons in comparison to all available 3D reconstructions in C. elegans (WHITE *et al.* 1986; BRITTIN *et al.* 2021; WITVLIET *et al.* 2021).

Machine learning assumptions, selection, performance

Our methodology for assumptions, selection, and performance of classification algorithms was used as previously described (COOK *et al.* 2023). In brief, we classify each edge (pairs of neurons known to be adjacent) as a binary value for synaptic weight (>0 average connection size = 1, no connection observed across samples = 0). We then trained our model using *C. elegans* adjacency and connectivity data using the mean scaled and normalized adjacency of pairs and a categorical variable describing whether two neurons are in the same or different strata (BRITTIN *et al.* 2021). Our models (MLPClassifier, DecisionTreeClassifier, RandomForestClassifier, and LogisticRegression from the scikit-learn library (PEDREGOSA *et al.* 2011) were then evaluated on the test dataset of *P. pacificus* adjacency and connectivity data. For comparative purposes, we again chose the parameters previously used in our logistic regression model for evaluating *C. elegans* adjacency and connectivity data.

Visualizing morphology and circuitry

Renderings of individual neurons or groups of neurons from Specimen 104 were performed using Adobe Dimension or Blender. Some post-rendering modifications of images were done with GraphicConverter. All code required to automate the processing of Blender

data are available at https://github.com/stevenjcook/cook_et_al_2024_mipristionchus. Individual neuron renderings, Blender and Adobe Dimension files used for rendering will be made available on Zenodo upon publication.

Circuit diagrams for individual neuron classes were generated using GraphViz (https://graphviz.org/) using the 'circo' layout. Display layouts of complete networks were made using Cytoscape (SMOOT *et al.* 2011). The layout structure is an implementation of an affinity view popularized by (VARSHNEY *et al.* 2011).

Quantification and statistical analysis

The statistical analysis performed in this paper is a combination of python software packages which include Scikit-learn and SciPy. All information for individual statistical tests including test and p-values can be found in the figure legends, while summary statistics are reported in the main test.

4D-microscopy and lineage analysis

The method for 4D-microscopy was described previously (SCHNABEL et al. 1997). Modifications of this system are described in (SCHNABEL *et al.* 2006). All 4D recordings generated were analyzed using the Software Database SIMI©BioCell (SIMI Reality Motion Systems, Unterschleissheim, Germany; http://www.simi.com/)(SCHNABEL *et al.* 1997; SCHNABEL *et al.* 2006). Cells are followed by the observer and the coordinates are recorded approximately every 2 min. The cell cleavages are assessed by marking the mother cell before the cleavage furrow ingresses and subsequently the centers of the daughter cells three frames later. By marking every cell during the complete embryonic development, the complete cell lineage of an embryo is generated.

Resource availability

This study did not generate new or unique reagents. All code and data necessary to perform the analyses in this paper are available at https://github.com/stevenjcook/cook_et_al_2024_pristionchus. Additional requests for information related to data analysis should be directed to SJC and OH.

Data Sources

C. elegans nerve ring connectivity and adjacency data were previously published

(COOK *et al.* 2019; BRITTIN *et al.* 2021; WITVLIET *et al.* 2021). The *P. pacificus* electron micrographs used in this study are previously published (BUMBARGER *et al.* 2013) and previously analyzed for amphidial circuitry (HONG *et al.* 2019).

ACKNOWLEDGEMENTS

This work was funded by the Howard Hughes Medical Institute. We thank Y. Ramadan, N. Schroeder, R. Hong, and M. Chalfie for discussions of *P. pacificus* gene expression, behavior and anatomy and David Hall, James Lightfoot, Nathan Schroeder, and members of the Hobert lab for comments on the manuscript.

AUTHOR CONTRIBUTIONS

SJC – conceptualization, methodology, investigation, formal analysis, software, writing, editing

CAK – investigation, formal analysis, software

CML – investigation, formal analysis, visualization, editing

NM – investigation, formal analysis

MM - investigation

SRS – investigation

DJB – conceptualization, methodology, investigation

MR – methodology, investigation

RS – investigation, formal analysis

RJS – editing, supervision, funding acquisition

OH – conceptualization, investigation, writing, editing, funding acquisition, supervision

DECLARATION OF INTERESTS:

The authors declare no conflicts of interest.

FIGURE LEGENDS

Figure 1: The reconstructed *Pristionchus pacificus* brain.

A: Left lateral view 3D rendering of all *P. pacificus* neurons reconstructed from all the analyzed serial micrographs of the head. Neurons are shown in different colors for contrast, the pharynx is indicated in teal.

B: Left lateral view 3D rendering of all neuronal nuclei in the *P. pacificus* head. Nuclei are colored by neuronal function: Sensory – red, interneuron – yellow, motor – blue.

C: Differential interference contrast image of *P. pacificus* embryo, indicating dying progenitor cell responsible for AVH neuron loss. See Figure 1 Supplement 2 for detailed lineage data.

D: Lineaging diagram displaying the death of AVH's sister cell in *C. elegans* (left) and AVH's progenitor cell death in *P. pacificus* (right) during embryogenesis. See Figure 1 Supplement 2 for detailed lineage data.

Figure 1 - SUPPLEMENT 1: 3D renderings of all reconstructed individual neurons.

3D renderings from 'Series 14' of all reconstructed individual *P. pacificus* neurons, each named for the presumptive *C. elegans* homologous neuron. Most neurons are shown with their bilateral homolog, each in a different color. In one case, a dorsal – ventral pair is shown (RMED, RMEV). Two sets of 6-fold symmetric cells are shown together (IL1s, IL2s). Unpaired neurons are shown alone. All head neurons are shown rendered in multiple views (see below) and colors; neuron colors have no particular meaning, except that the different colors of bilaterally paired neurons were chosen to make the two neurons and their neurites distinguishable from each other. As a constant landmark, the pharynx is shown in light green. Disrupted neuron trajectories in the posterior reflect that the serial section electron micrograph series ends within the retrovesicular ganglion. In all images, anterior is to the left. Viewpoints, top to bottom; views 1 – 4 views are rotated ~90° each step approximately around the pharyngeal center on the anterior-posterior axis: 1. Left lateral (top), 2. Dorsal, 3. Right lateral, 4. Ventral, 5. Rear, left side (bottom), anterior to the upper left. For both left (1) and right (3) lateral views, the view is slightly tilted relative to being precisely lateral, to better show the opposite bilateral homolog for paired neurons. The relative 'zoom' of different renderings varies to show the complete set of neurites and/or soma locations. The viewpoints are most 'zoomed out' for cells with somas and/or neurites in the retrovesicular ganglion. Rendered with Adobe Dimension. Some post-rendering retouching performed with Graphic

Converter, especially changing background grey to enhance edge contrast.

Figure 1 - SUPPLEMENT 2: AVHR progenitor death in *P. pacificus,* compared to *C. elegans.*

Primary lineage data generated by Simi BioCell is shown. Cell fates are defined by nuclear morphology (N= neuron-like nuclear morphology; D = cell death; U = muscle; M= mitosis; P = pharynx; H = hypodermal; duplicated letter means: first letter = predicted fate; second letter = actually observed fate).

A: Lineage data for the *P. pacificus* embryo, showing the death of AVHL/R's mother cell.

B: Lineage data for *C. elegans* embryo, highlighting AVHL/R.

C: Phylogenetic tree of the PAS domain of bHLH-PAS proteins from various nematode species, illustrating loss of *hlh-34* in *P. pacificus* (blue) vs *C. elegans* (red).

Figure 1 - SUPPLEMENT 3: g2 progenitor death in *P. pacificus,* compared to *C. elegans.*

Primary lineage data generated by Simi BioCell is shown. Cell fates are defined by nuclear morphology (See previous legend for meaning of letter code).

A: Lineage data for the *P. pacificus* embryo, showing the death of g2L's mother cell.

B: Lineage data for *C. elegans* embryo, highlighting the death of g2L's sister cell.

C: Schematic lineage diagram depicting the death of g2L's mother cell in *P. pacificus*.

D: Schematic lineage diagram depicting the death of g2L's sister cell in *C. elegans.*

Figure 1 - SUPPLEMENT 4: AVHL and g2 survival in *Acrobeloides nanus* and *Plectus sambesii.*

Primary lineage data generated by Simi BioCell is shown. Cell fates are defined by nuclear morphology (See previous legend for meaning of letter code).

Figure 1 - SUPPLEMENT 5: Anterior displacement of the IL2 neurons. Shown is a rendering of the dorsal IL2 neuron pair (black). Its axons are closely fasciculated with the sensory dendrites and then axons of the IL1 neuron pair (orange). The IL2 somas are nestled in between the IL socket (blue) and sheath (magenta) glia somas.

Figure 2: Morphological evolution of neurite trajectories.

In each panel (**A-E**), the top section shows a schematic comparison of the neuron's morphology in *C. elegans* (red) and *P. pacificus* (blue). Schematics are left lateral views (anterior to the left and dorsal up) for all panels except **C** (AQR), which is a ventral view. The pharynx is shown in green and the nerve ring (neuropil region) is grey, outlined by a dashed line. Below the schematics are a connectivity diagram and 3D rendering of the *P. pacificus* neuron (blue), in some cases with a partner neuron (magenta). Connectivity diagrams show chemical synapses that are conserved in all adult nematode samples (black), are *C. elegans*-specific (red), or *P. pacificus*-specific (blue). Line width is proportional to synaptic weight and arrowhead shows directionality. (A connectivity diagram in not relevant for panel E, so is not included there.)

A: URB morphology*,* illustrating the absence of dendrite in *P. pacificus.* The 3D rendering of *P. pacificus* URB (blue) is shown with a conserved synaptic partner of URB, the inner labial sensory neuron IL1 (magenta), which retains its dendrite in *P. pacificus*, extending from the nerve ring region to beyond the anterior tip of the pharynx.

B: PVD morphology*,* illustrating that in *P. pacificus* PVD extends into the nerve ring where it synapses with AVJ and AVD (seen in in both *P. pacificus* samples). Double slash indicates the PVD soma is posterior to the reconstruction. 3D rendering shows PVD (blue) with *P. pacificus*-specific synaptic partner AVD (magenta), a closeup of the nerve ring region.

C: RIP morphology*,* illustrating extended nerve ring neurites in *P. pacificus.* 3D rendering shows RIP (blue) together with *P. pacificus*-specific synaptic partner AIZ (magenta), a closeup of the nerve ring region.

D: AQR morphology *(ventral view),* illustrating how the *P. pacificus* AQR neuron crosses over the dorsal midline rather than bifurcating ventrally as seen in *C. elegans*. 3D rendering shows AQR (blue) entering nerve ring on the left (top), extending over dorsally to the right side (bottom). The AQR dendrite extends along the right side (bottom) almost to the nerve ring. Dashed line indicates that the posterior-most AQR connecting neurite is not included in the reconstruction.

E. ASJ morphology, illustrating branches protruding from or nearby the ASJ soma in *P. pacificu*s not found in *C. elegans*. 3D renderings of both ASJL (blue) and ASJR (magenta) are shown in lateral posterior view (left) and dorsal posterior view (right, with nearly transparent pharynx), showing that these branches, indicated by arrows, project near the pseudocoelom.

F. AVM and ALM morphologies, illustrating that in *P. pacificus,* AVM does not send a neurite into the nerve ring (where in *C. elegans* it forms a gap junction with ALM). Instead, ALM extends a neurite to meet ALM ventrally, where it then forms a gap junction in this location. Double slash indicates the AVM and ALM somas are posterior to the reconstruction. 3D rendering shows simpler *P. pacificus* AVM neurite (blue) contacted by extended ALM neurite (magenta). Connectivity diagram shows many *C. elegans*-specific synapses made in the nerve ring by AVM, which no longer contacts these cells in *P. pacificus.*

Figure 2 - Supplement 1: Ultrastructural details of anatomical differences.

A: EM micrograph showing URB NMJs. Active zones are shown with asterisks.

B: EM micrograph showing PVD's synaptic output onto the AVJ and AVD neurons. Active zones are shown with asterisks.

C: EM micrograph showing dense core vesicles within ASJ's species-specific perisomatic branch.

D: EM micrograph showing a chemical synapse (left asterisk) and gap junction (right asterisk) along AVM's microtubule process.

Figure 3: Chemical synaptic connectome comparison across species.

Panels A-D: Network (wiring) diagrams showing all neurons in the nerve ring and their synaptic connections: core (black), variable (gray), *P. pacificus*-specific (blue), *C. elegans*-specific (red).

Sensory, inter-, and motor neurons are represented by triangles, octagons, and squares, respectively. Arrow widths are proportional to the average number of synapses across datasets; arrowheads represent directionality.

A. Complete wiring diagram showing all *P. pacificus* and *C. elegans* connections.

B. Core wiring diagram highlighting shared, non-variable connections.

C. Diagram highlighting *P. pacificus*-specific connections.

D. Diagram highlighting *C. elegans*-specific connections.

Figure 3 – Supplement 1: Analysis of species-specific undirected chemical synapses by class across development.

All embryonically born sex-shared nerve ring neurons that make a species-specific synaptic connection are shown.

A) Stacked bar graphs of the fraction of species-specific synaptic connections relative to all other synapses made by the respective neuron class.

B) Stacked bar graphs of the number of sex-specific inputs and outputs by neuron class.

Figure 3 – Supplement 2: Directed connectivity of all head neurons shown individually.

Figure 4: Neurite neighborhood shifts and quantitative analysis of synaptic connectivity differences.

A: Schematic comparison of ASH neuron morphology in *C. elegans (red)* and *P. pacificus (blue),* showing similar morphology from this viewpoint. Left lateral view (see legend for Fig 2).

B: Schematic of nerve ring cross section showing lateral displacement of ASH neurite in *P. pacificus* (blue) compared to *C. elegans* (red). The shift in neighborhood is shown in a diagram as a driver of synaptic rewiring.

C: Adult wiring diagram of ASH.

D: Histogram of adjacency conservation among all nematode nerve ring series (*C. elegans*-specific edges are red, *P. pacificus*-specific edges are blue, core edges are black, and variable edges are gray).

E: Histogram of connectivity conservation among all nematode nerve ring series.

F: Histogram of adjacency conservation among adult nerve ring series.

G: Histogram of connectivity conservation among adult nerve ring series.

H. Violin plot comparing mean scaled adjacency and connectivity specificity classification Condition: not specific, U statistic: 733073.5, Corrected p-value: 2.46e-27 Condition: none, U statistic: 860516.5, Corrected p-value: 6.56e-109 Condition: core, U statistic: 12093.0, Corrected p-value: 3.14e-14 Condition: *P.* pacificus-specific, U statistic: 5257.0, Corrected p-value: 1.60e-06 Condition: *C. elegans*-specific, U statistic: 180.0, Corrected p-value: 8.40e-04.

I. Violin plot comparing log+1 adjusted number of synapses and connectivity specificity classification. Condition: not specific, U statistic: 1803223.0, Corrected p-value: 7.23e-36 Condition: core, U statistic: 7903.0, Corrected p-value: 1.00e+00 Condition: *P. pacificus*-specific, U statistic: 0.0, Corrected p-value: 3.08e-49 Condition: *C. elegans*-specific, U statistic: 12100.0, Corrected p-value: 4.06e-42.

For underlying data, see **Supplement Data 5 and 6**.

Figure 4 - Supplement 1: Characteristics of adult synaptic connectivity.

A: Bar graphs of adult directed synaptic connectivity classification vs adjacency classification.

B: Histograms of the count of synapses faceted by synaptic classification among adult series.

Figure 4 - Supplement 2: Neuronal adjacency predicts connectivity in *P. pacificus.*

A. Red scatter plot of the mean scaled adjacency vs. mean connection strength for neuron pairs in the same strata. Regression line is shown in red, Spearman's r = 0.750

B. Blue scatter plot of mean scaled adjacency vs. Mean connection strength for neuron pairs in different strata. Regression line is shown in blue, Spearman's r = 0.726.

C. Table of 10-fold cross-validation of Multi-layer Perceptron, Random Forest, Decision Tree, and Logistic Regression classification algorithm results.

D. Receiver operator curves of cross-validated model (kfolds = 10). The black line and gray area are the mean (0.86) and standard deviation (0.04), respectively.

D. Precision recall curves of cross-validated model (kfolds = 10). The black line and gray area are the mean (0.87) and standard deviation (0.04), respectively.

Figure 5: Glial rewiring across species.

A: Lateral posterior view of 3D rendering of IL sheath and socket cell

B: Lateral posterior view of 3D rendering of the CEPshDL and AWCL cells.

C: Posterior view rendering of CEPshDL/R and AWC cells.

D: Chemical synaptic connectivity of CEPsh in adults. Blue lines are connections found only in *P. pacificus*, red lines are connections found only in *C. elegans*, and black lines are connections found in both species.

E: Lateral posterior view rendering of 3D reconstruction of the GLR cells.

F: Posterior lateral view of the GLRL and RIPL cells, showing close fasciculation of processes.

G: Region of synaptic output of GLR cells (pink) with an EM micrograph showing presynaptic specializations within the GLR cell

H: Chemical synaptic connectivity of GLR in adults. Blue lines are connections found only in *P. pacificus*, red lines are connections found only in *C. elegans*, and black lines are connections found in both species.

SUPPLEMENT DATA

Supplement Data 1: Neuronal adjacencies within the nerve ring of Specimen 107.

Supplement Data 2: Neuronal adjacencies within the nerve ring of Specimen 148.

Supplement Data 3: Connectivity of *P. pacificus* reconstruction from Specimen 107

Supplement Data 4: Connectivity of *P. pacificus* reconstruction from Specimen 148.

Supplement Data 5: Composite dataset of undirected adjacency and connectivity across nematode samples

Supplement Data 6: Composite dataset of directed adult chemical connectivity across nematode samples.

REFERENCES

Athanasouli, M., H. Witte, C. Weiler, T. Loschko, G. Eberhardt *et al.*, 2020 Comparative genomics and community curation further improve gene annotations in the nematode Pristionchus pacificus. BMC Genomics 21**:** 708.

Berghoff, E. G., L. Glenwinkel, A. Bhattacharya, H. Sun, E. Varol *et al.*, 2021 The Prop1-like homeobox gene unc-42 specifies the identity of synaptically connected neurons. Elife 10.

Brittin, C. A., S. J. Cook, D. H. Hall, S. W. Emmons and N. Cohen, 2021 A multi-scale brain map derived from whole-brain volumetric reconstructions. Nature 591**:** 105-110.

Bumbarger, D. J., M. Riebesell, C. Rödelsperger and R. J. Sommer, 2013 System-wide rewiring underlies behavioral differences in predatory and bacterial-feeding nematodes. Cell 152**:** 109-119.

Cardona, A., S. Saalfeld, J. Schindelin, I. Arganda-Carreras, S. Preibisch *et al.*, 2012 TrakEM2 Software for Neural Circuit Reconstruction. PloS ONE 7**:** e38011-e38011.

Chalfie, M., J. E. Sulston, J. G. White, E. Southgate, J. N. Thomson *et al.*, 1985 The neural circuit for touch sensitivity in Caenorhabditis elegans. J Neurosci 5**:** 956-964.

Cook, S. J., T. A. Jarrell, C. A. Brittin, Y. Wang, A. E. Bloniarz *et al.*, 2019 Whole-animal connectomes of both Caenorhabditis elegans sexes. Nature 571**:** 63-71.

Cook, S. J., C. A. Kalinski and O. Hobert, 2023 Neuronal contact predicts connectivity in the C. elegans brain. Curr Biol 33**:** 2315-2320 e2312.

Cook, S. J., B. Vidal and O. Hobert, 2021 The bHLH-PAS gene hlh-34 is expressed in the AVH, not AVJ interneurons. MicroPubl Biol 2021.

Eizinger, A., B. Jungblut and R. J. Sommer, 1999 Evolutionary change in the functional specificity of genes. Trends Genet 15**:** 197-202.

Frakes, A. E., M. G. Metcalf, S. U. Tronnes, R. Bar-Ziv, J. Durieux *et al.*, 2020 Four glial cells regulate ER stress resistance and longevity via neuropeptide signaling in C. elegans. Science 367**:** 436-440.

Fricker, M., A. M. Tolkovsky, V. Borutaite, M. Coleman and G. C. Brown, 2018 Neuronal Cell Death. Physiol Rev 98**:** 813-880.

Hengartner, M. O., and H. R. Horvitz, 1994 Programmed cell death in Caenorhabditis elegans. Curr Opin Genet Dev 4**:** 581-586.

Hong, R. L., M. Riebesell, D. J. Bumbarger, S. J. Cook, H. R. Carstensen *et al.*, 2019 Evolution of neuronal anatomy and circuitry in two highly divergent nematode species. Elife 8.

Hong, R. L., and R. J. Sommer, 2006 Chemoattraction in Pristionchus nematodes and implications for insect recognition. Curr Biol 16**:** 2359-2365.

Kaplan, J. M., and H. R. Horvitz, 1993 A dual mechanosensory and chemosensory neuron in Caenorhabditis elegans. Proc Natl Acad Sci U S A 90**:** 2227-2231.

Katz, P. S., 2016 Evolution of central pattern generators and rhythmic behaviours. Philos Trans R Soc Lond B Biol Sci 371**:** 20150057.

Kroetz, S. M., J. Srinivasan, J. Yaghoobian, P. W. Sternberg and R. L. Hong, 2012 The cGMP signaling pathway affects feeding behavior in the necromenic nematode Pristionchus pacificus. PLoS One 7**:** e34464.

Lee, H., M. K. Choi, D. Lee, H. S. Kim, H. Hwang *et al.*, 2012 Nictation, a dispersal behavior of the nematode Caenorhabditis elegans, is regulated by IL2 neurons. Nat Neurosci 15**:** 107-112.

Lightfoot, J. W., M. Wilecki, C. Rodelsperger, E. Moreno, V. Susoy *et al.*, 2019 Small peptide-mediated self-recognition prevents cannibalism in predatory nematodes. Science 364**:** 86-89.

Loer, C. M., and L. Rivard, 2007 Evolution of neuronal patterning in free-living rhabditid nematodes I: Sex-specific serotonin-containing neurons. J Comp Neurol 502**:** 736-767.

Moreno, E., A. McGaughran, C. Rodelsperger, M. Zimmer and R. J. Sommer, 2016 Oxygen-induced social behaviours in Pristionchus pacificus have a distinct evolutionary history and genetic regulation from Caenorhabditis elegans. Proc Biol Sci 283**:** 20152263.

Pedregosa, F., G. Varoquaux, A. Gramfort, V. Michel, B. Thirion *et al.*, 2011 Scikit-learn: Machine learning in Python. the Journal of machine Learning research 12**:** 2825-2830.

Qing, X., Y. M. Zhang, S. Sun, M. Ahmed, W. S. Lo *et al.*, 2023 Phylogenomic Insights into the Evolution and Origin of Nematoda. bioRxiv.

Ragsdale, E. J., M. R. Muller, C. Rodelsperger and R. J. Sommer, 2013 A developmental switch coupled to the evolution of plasticity acts through a sulfatase. Cell 155**:** 922-933.

Riebesell, M., and R. J. Sommer, 2017 Three-dimensional reconstruction of the pharyngeal gland cells in the predatory nematode Pristionchus pacificus. J Morphol 278**:** 1656-1666.

Roberts, R. J. V., S. Pop and L. L. Prieto-Godino, 2022 Evolution of central neural circuits: state of the art and perspectives. Nat Rev Neurosci 23**:** 725-743.

Savtchouk, I., and A. Volterra, 2018 Gliotransmission: Beyond Black-and-White. J Neurosci 38**:** 14-25.

Schnabel, R., M. Bischoff, A. Hintze, A. K. Schulz, A. Hejnol *et al.*, 2006 Global cell sorting in the C. elegans embryo defines a new mechanism for pattern formation. Dev Biol 294**:** 418-431.

Schnabel, R., H. Hutter, D. Moerman and H. Schnabel, 1997 Assessing normal embryogenesis in Caenorhabditis elegans using a 4D microscope: variability of development and regional specification. Dev Biol 184**:** 234-265.

Schroeder, N. E., R. J. Androwski, A. Rashid, H. Lee, J. Lee *et al.*, 2013 Dauer-specific dendrite arborization in C. elegans is regulated by KPC-1/Furin. Curr Biol 23**:** 1527-1535.

Smoot, M. E., K. Ono, J. Ruscheinski, P.-L. Wang and T. Ideker, 2011 Cytoscape 2.8: new features for data integration and network visualization. Bioinformatics (Oxford, England) 27**:** 431-432.

Srinivasan, J., O. Durak and P. W. Sternberg, 2008 Evolution of a polymodal sensory response network. BMC Biol 6**:** 52.

Sulston, J. E., E. Schierenberg, J. G. White and J. N. Thomson, 1983 The embryonic cell lineage of the nematode Caenorhabditis elegans. Dev Biol 100**:** 64-119.

True, J. R., and E. S. Haag, 2001 Developmental system drift and flexibility in evolutionary trajectories. Evol Dev 3**:** 109-119.

Varshney, L. R., B. L. Chen, E. Paniagua, D. H. Hall and D. B. Chklovskii, 2011 Structural properties of the Caenorhabditis elegans neuronal network. PLoS Comput Biol 7**:** e1001066.

White, J. G., E. Southgate, J. N. Thomson and S. Brenner, 1986 The structure of the nervous system of the nematode *Caenorhabditis elegans*. Philosophical Transactions of the Royal Society of London B. Biological Sciences 314**:** 1-340.

Witvliet, D., B. Mulcahy, J. K. Mitchell, Y. Meirovitch, D. R. Berger *et al.*, 2021 Connectomes across development reveal principles of brain maturation. Nature 596**:** 257-261.

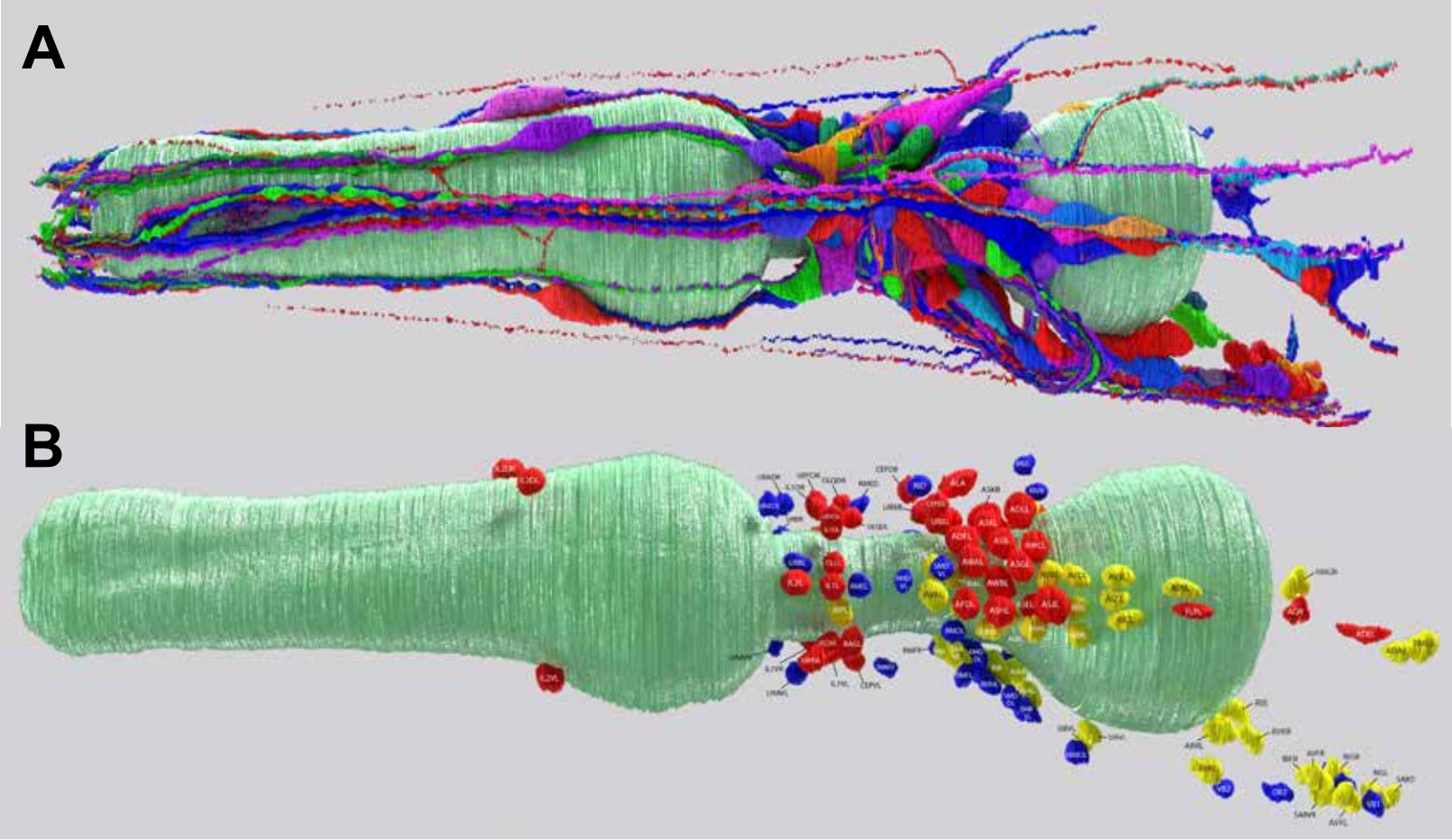
A
B

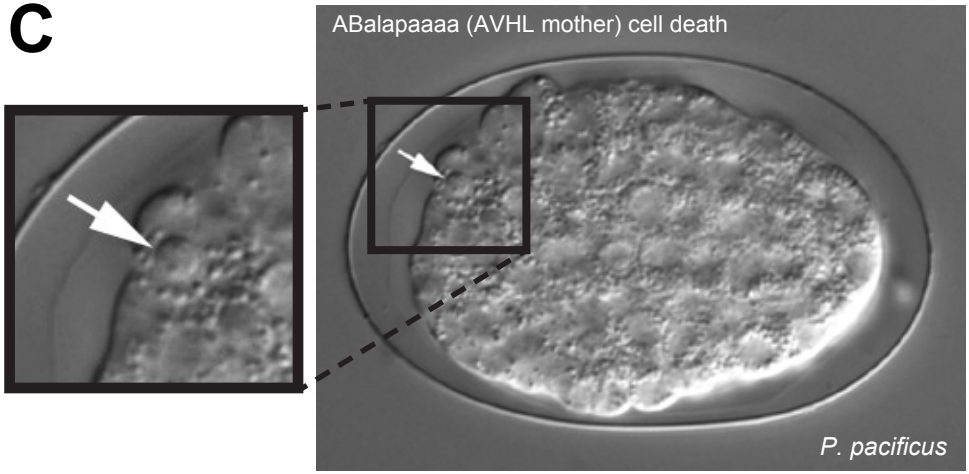
C
ABalapaaaa (AVHL mother) cell death
P. pacificus

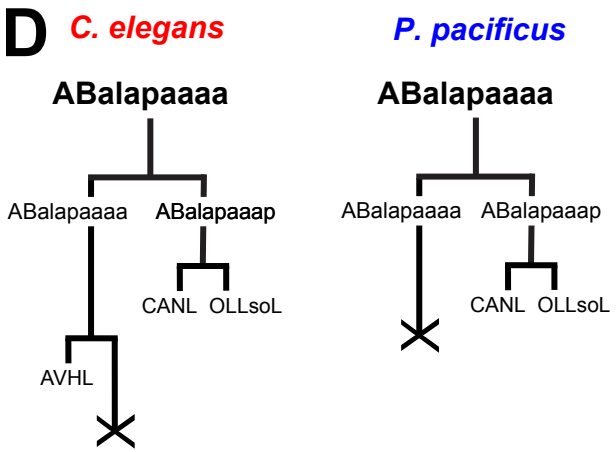
D
C. elegans
P. pacificus
ABalapaaaa
ABalapaaaa
ABalapaaap
CANL
OLLsoL
AVHL
ABalapaaaa
ABalapaaaa
ABalapaaap
CANL
OLLsoL

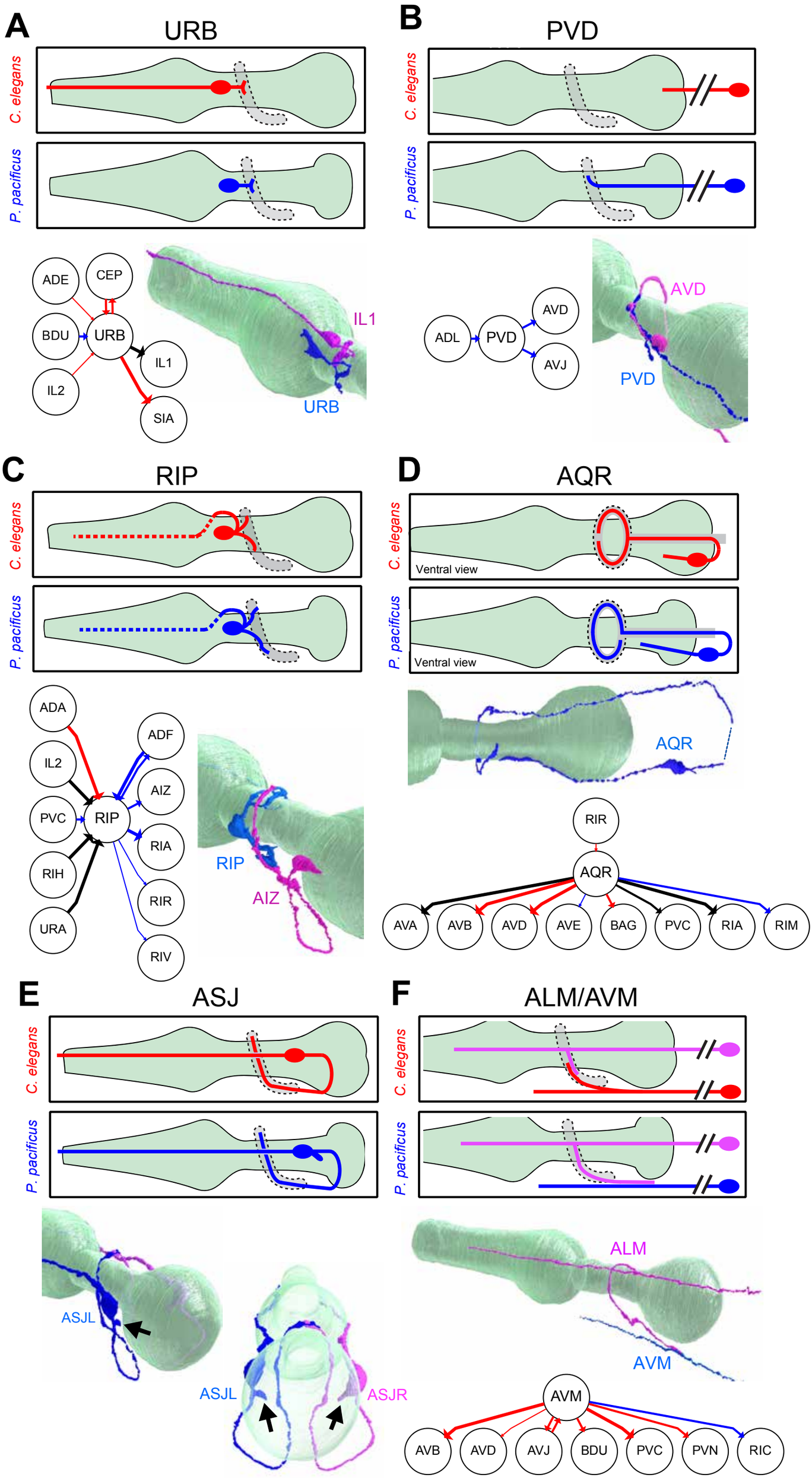
A
URB
C. elegans
P. pacificus
ADE
CEP
BDU
URB
IL1
IL2
SIA
IL1
URB
B
PVD
C. elegans
P. pacificus
ADL
PVD
AVD
AVJ
AVD
PVD
C
RIP
C. elegans
P. pacificus
ADA
ADF
IL2
AIZ
PVC
RIP
RIA
RIH
RIR
URA
RIV
RIP
AIZ
D
AQR
C. elegans
P. pacificus
Ventral view
Ventral view
AQR
RIR
AQR
AVA
AVB
AVD
AVE
BAG
PVC
RIA
RIM
E
ASJ
C. elegans
P. pacificus
ASJL
ASJL
ASJR
F
ALM/AVM
C. elegans
P. pacificus
ALM
AVM
AVM
AVB
AVD
AVJ
BDU
PVC
PVN
RIC

Fig 2

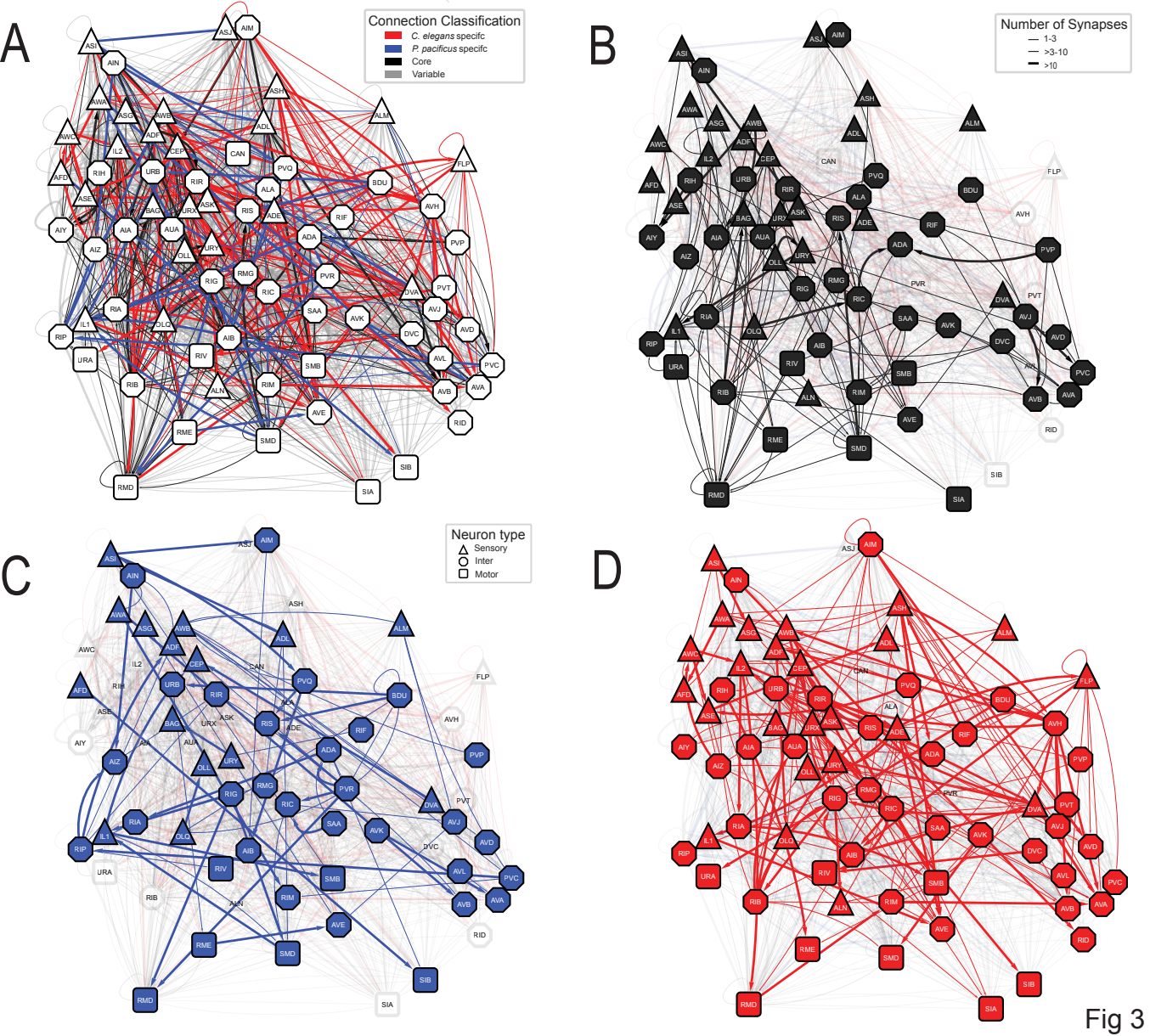
A
Connection Classification
C. elegans specifc
P. pacificus specifc
Core
Variable
B
Number of Synapses
1-3
>3-10
>10
C
Neuron type
Sensory
Inter
Motor
D
ASJ
AIM
ASI
AIN
ASH
AWA
ASG
AWB
ADL
ALM
AWC
ADF
IL2
CEP
CAN
PVQ
FLP
AFD
RIH
URB
RIR
ALA
BDU
ASE
BAG
URX
ASK
RIS
ADE
RIF
AVH
AIY
AIA
AUA
ADA
PVP
AIZ
OLL
URY
RIG
RMG
PVR
RIC
DVA
PVT
RIA
SAA
AVJ
IL1
OLQ
AVK
AVD
RIP
AIB
DVC
RIV
SMB
AVL
PVC
URA
RIB
ALN
RIM
AVB
AVA
AVE
RID
RME
SMD
SIB
RMD
SIA

Fig 3

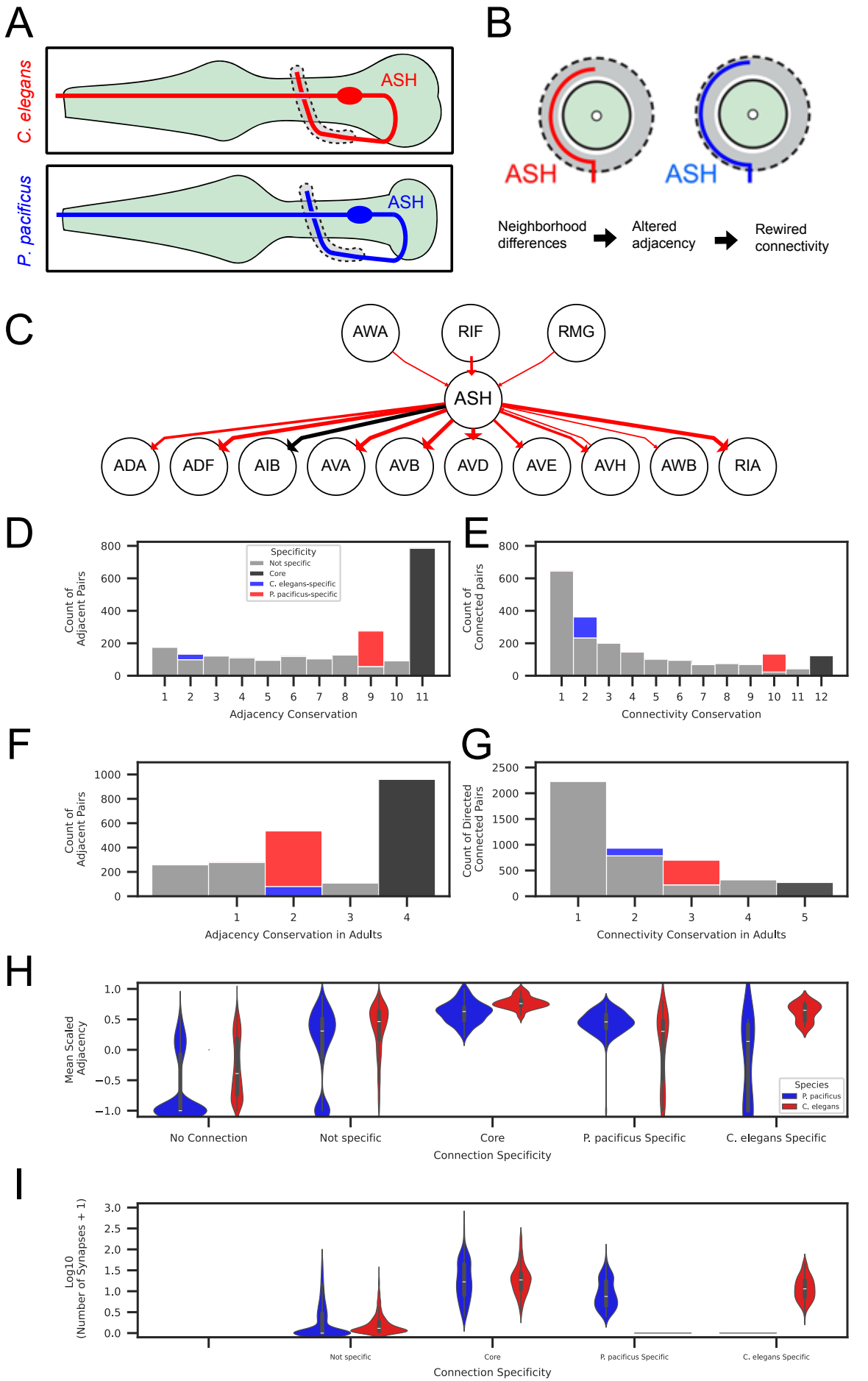
A
C. elegans
ASH
P. pacificus
ASH
B
ASH
ASH
Neighborhood differences
Altered adjacency
Rewired connectivity
C
AWA
RIF
RMG
ASH
ADA
ADF
AIB
AVA
AVB
AVD
AVE
AVH
AWB
RIA
D
Count of Adjacent Pairs
Specificity
Not specific
Core
C. elegans-specific
P. pacificus-specific
Adjacency Conservation
E
Count of Connected pairs
Connectivity Conservation
F
Count of Adjacent Pairs
Adjacency Conservation in Adults
G
Count of Directed Connected Pairs
Connectivity Conservation in Adults
H
Mean Scaled Adjacency
Species
P. pacificus
C. elegans
No Connection
Not specific
Core
P. pacificus Specific
C. elegans Specific
Connection Specificity
I
Log10 (Number of Synapses + 1)
Not specific
Core
P. pacificus Specific
C. elegans Specific
Connection Specificity

Fig 4

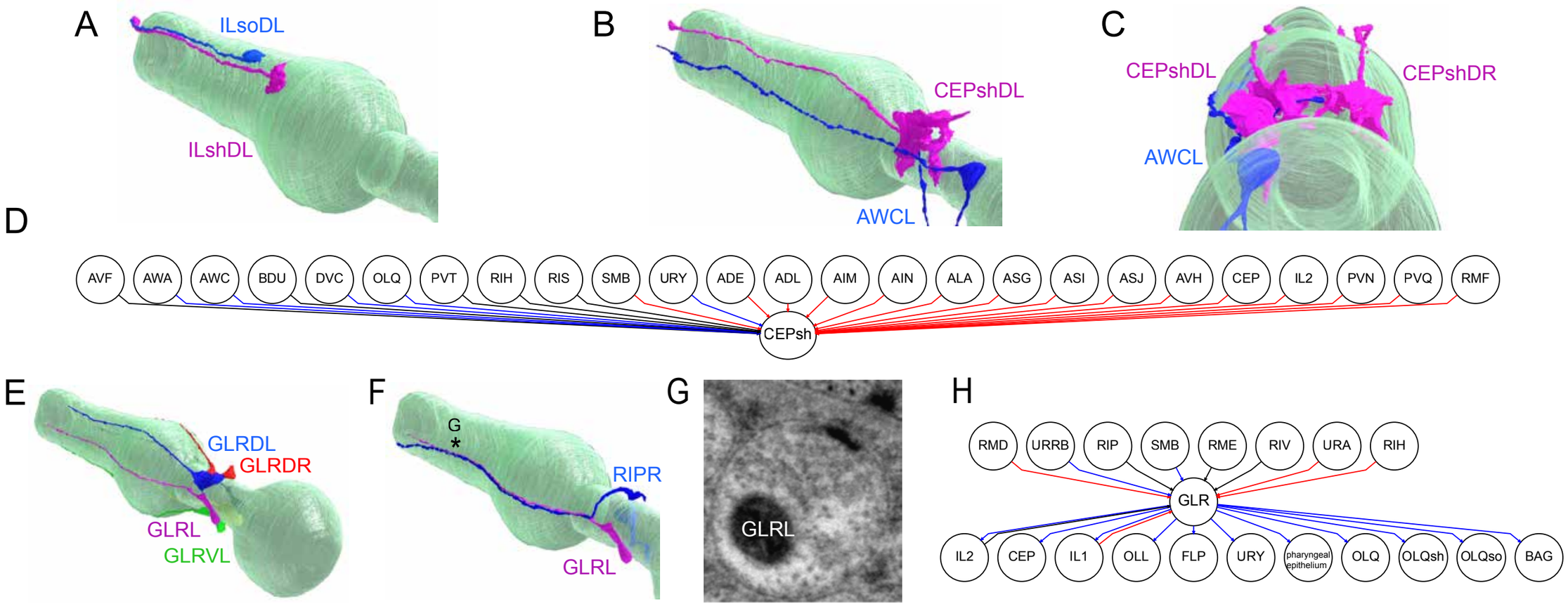
A
ILsoDL
ILshDL
B
CEPshDL
AWCL
C
CEPshDL
CEPshDR
AWCL
D
AVF
AWA
AWC
BDU
DVC
OLQ
PVT
RIH
RIS
SMB
URY
ADE
ADL
AIM
AIN
ALA
ASG
ASI
ASJ
AVH
CEP
IL2
PVN
PVQ
RMF
CEPsh
E
GLRDL
GLRDR
GLRL
GLRVL
F
G
*
RIPR
GLRL
G
GLRL
H
RMD
URRB
RIP
SMB
RME
RIV
URA
RIH
GLR
IL2
CEP
IL1
OLL
FLP
URY
pharyngeal epithelium
OLQ
OLQsh
OLQso
BAG

Fig 5